Position converted to R1	Cα-Cα distance (nm)	Backbone structural environment
H3V46	5.1	Start of αN-helix
H3R49	5.1	αN-helix
H3L65	6.3	Start of α1-helix
H3Q76	5.9	end of α1-helix
H3M90	4.8	α2-helix
H3Q125	1.8*	α3-helix
H4N25	5.9	Start of αN-helix
H4T30	5.3	loop between αN and α1 helices
H4R45	3.2	β-sheet between α1 and α2 helices
H4S47	3.2	α2 helix
H4L49	3.6	Start of a2-helix
H4V60	3.4	α2-helix
H4E63	3.9	α2-helix
H4R67	3.8	α2-helix
H4T71	3.8	α2-helix
H4T82	4.4	Between β-sheet and α3 helix

Supplementary Table S1: List of mutants prepared showing Cα-Cα distances and secondary structural environment (taken from 1TZY) Cα-Cα distance less than 2 nm, but spin label position predicted to be longer.

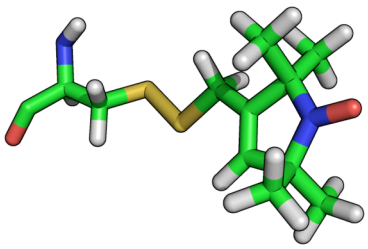

Supplementary figure S1: Structure of R1 side chain (or reaction of cysteine with MTSL)

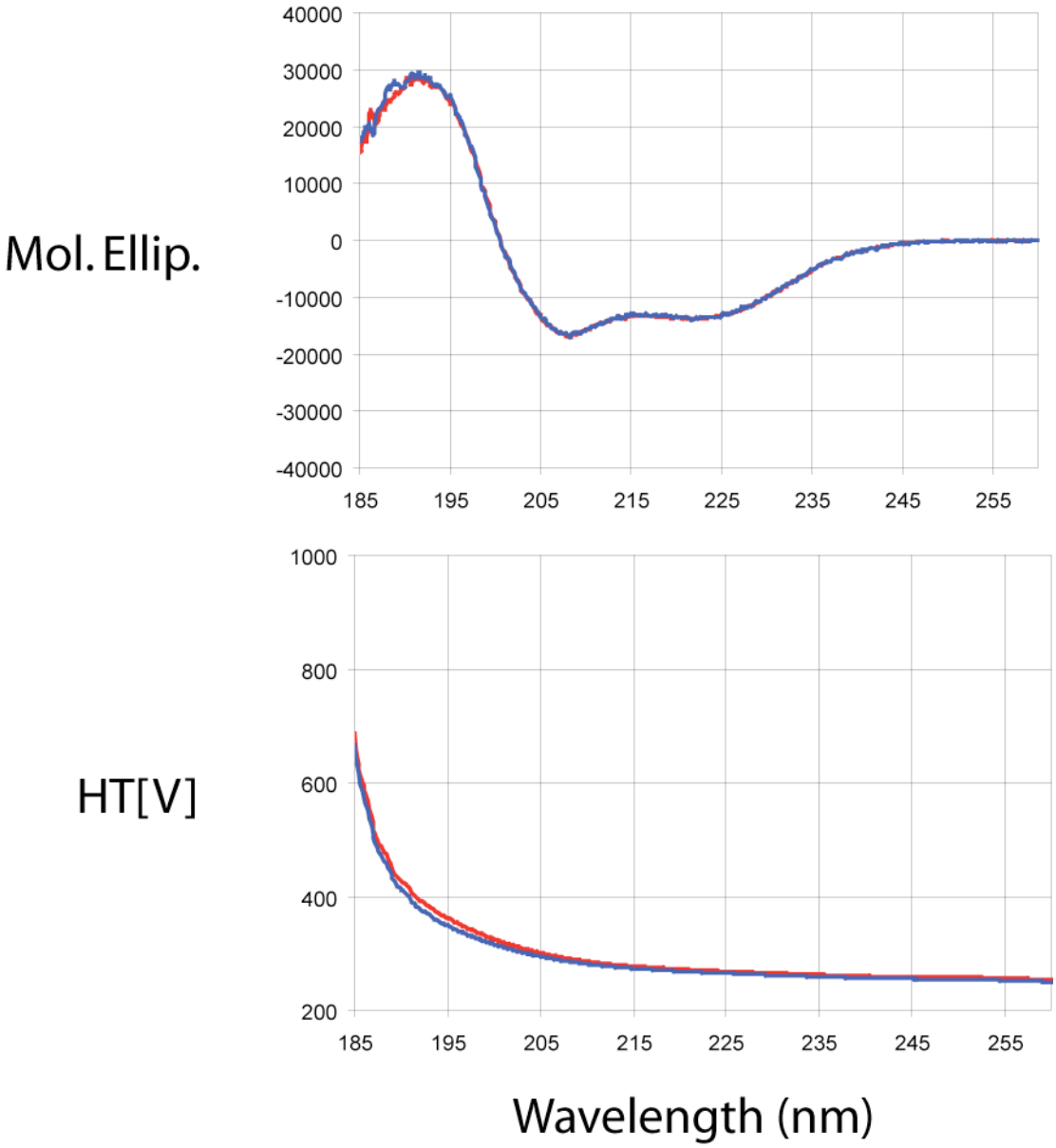

Supplementary figure S2: Far UV circular dichroism spectra of H3C110A/H4wt (blue) and H3C110A/H4E63C (red). The spectrum from H4E63C is virtually superimposable on the H4wt, indicating no gross structural pertubation associated with this mutation.

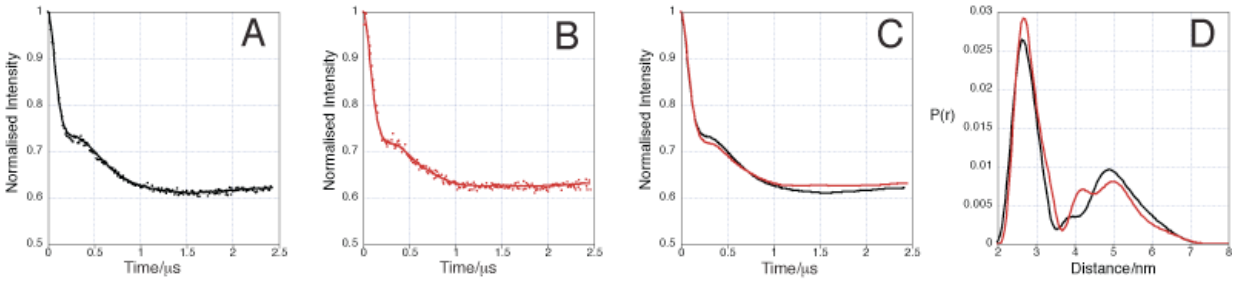

Supplementary figure S3: PELDOR data for H4S47R1 tetramer prepared using different salt concentrations.
A) Background corrected echo oscillation (black dots) and Tikhonov derived fit (black line) to PELDOR data for H4S47R1 tetramer prepared in high salt (1M NaCl).
B) Background corrected echo oscillation (red dots) and Tikhonov derived fit (red line) to PELDOR data for H4S47R1 tetramer prepared in low salt (0.1M NaCl).
C) Comparison of Tikhonov derived fits for H4S47R1 tetramer in 1M (black line) and 0.1M (red line) NaCl.
D) Tikhonov regularisation derived distance distributions for H4S47R1 tetramer in 1M NaCl (black) and 0.1M NaCl (red).

By preparing a sample of H4S47R1 tetramer in either 1M or 0.1M sodium chloride, the critical question of whether the H3-H4 tetramer is stable under physiological conditions (i.e. low salt) could be investigated, since only the tetramer will give rise to an observable dipolar coupling in the PELDOR experiment. Our data clearly demonstrate that a dipolar coupling is present from the sample prepared under low salt conditions. The oscillation depth measured in both samples is identical thus indicating that the tetramer is the predominant species at both high and low salt.

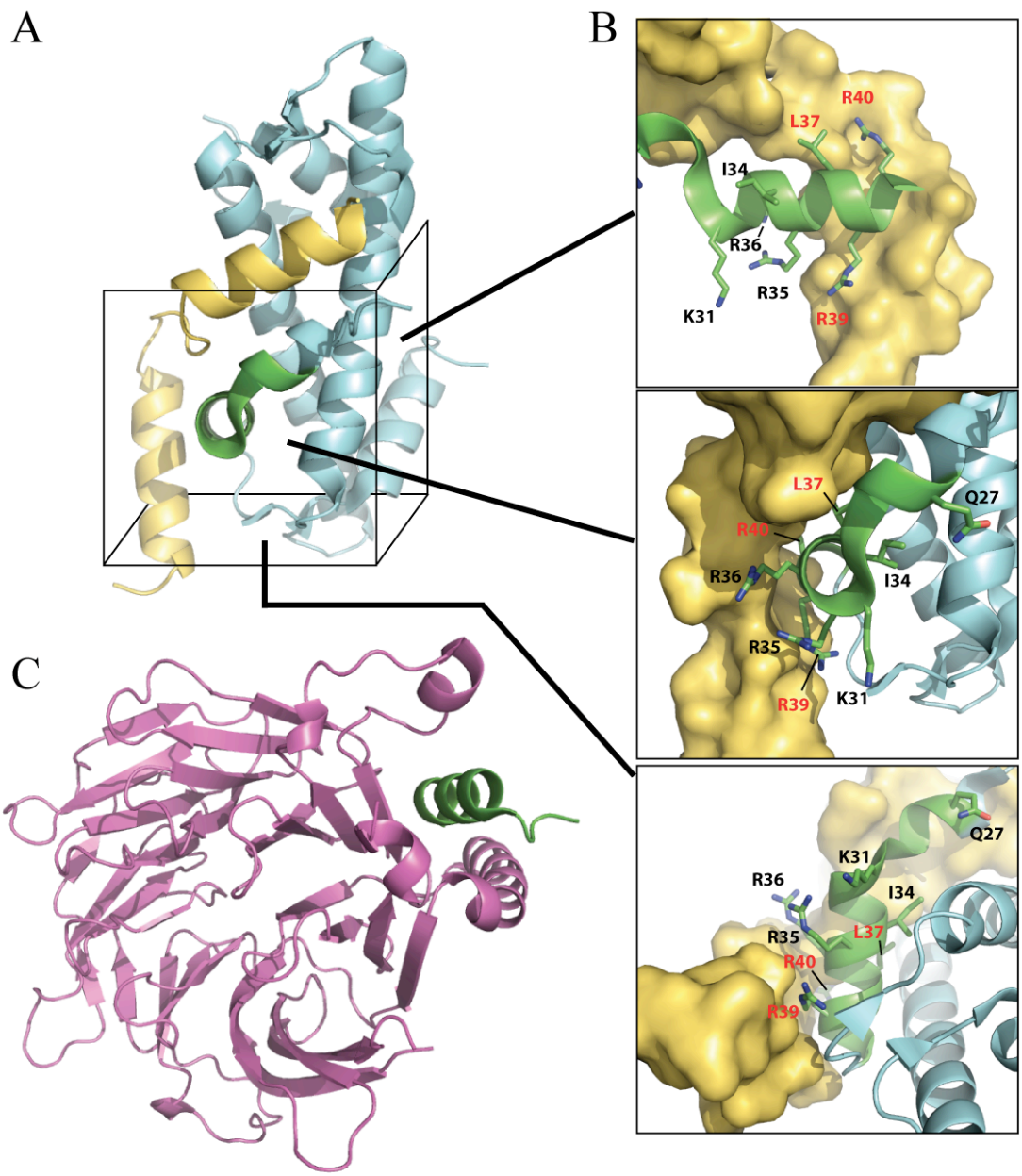

Supplementary figure S4: The H3 αN & α1 helix obscures residues critical for RbAp46 binding.
(A) An H3-H4 dimer extracted from the octamer crystal structure 1TZY. The H3 αN & α1 helix are shown in yellow, H4 α1 helix in green and the remainder of the dimer in light blue.
(B) Three alternate views of the region boxed in A. Side-chains of residues identified as being important for interaction with RbAp46 are represented as sticks. Those found to be particularly critical for binding, which are also obscured by the H3 αN & α1 helices, are shown in red. In the top panel the region shown in light blue in A is omitted for clarity.
(C) The crystal structure of RbAp46 (magenta) bound to the H4 α1 helix peptide (green) (PDB accession code 3CFS).In the crystal structure of the histone octamer the H4 α1 helix is obscured by the H3 αN helix, whereas in solution, without the stabilising effect of the H2A-H2B dimers, instability of the αN helix in the histone tetramer would allow access to the α1 helix of H4 by RbAp46/p55

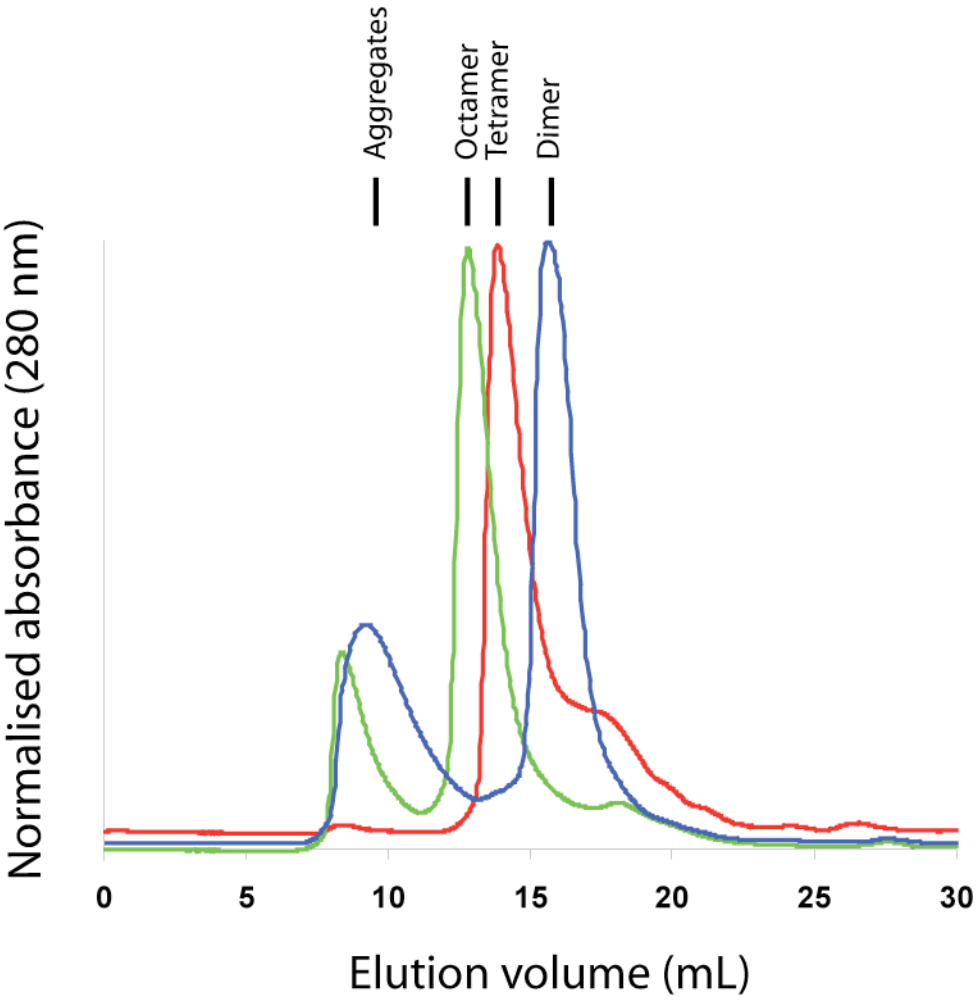

Supplementary figure S5
Typical elution profile from size exclusion chromatography of histone octamer (green) and tetramer (red) for mutant H4N25C:H3C110A on a 10/300 GL column packed with Superdex200 (GE Healthcare). As a comparison the elution for H2A-H2B dimers is also shown (blue). Misfolded aggregates eluted at 9-10 mL, histone octamer at ~12.8 mL, histone tetramer at ~13.8 mL and H2A-H2B dimers at 15.7 mL as shown.